JOURNAL OF THERMOPHYSICS AND HEAT TRANSFER
Vol. 23, No. 3, July–September 2009

Effects of Chemistry in Nonequilibrium Hypersonic Flow Around Blunt Bodies

Ghislain Tchuen*
Université de Dschang, Laboratoire d'Ingénierie des Systémes Industriels et de l'Environnement, Bandjoun, Cameroon
and
David E. Zeitoun†
Université de Provence, 13453 Marseille Cedex 13, France

DOI: 10.2514/1.42665

In this paper, the influence of a chemical kinetic model in hypersonic flow past blunt bodies is examined. Slow and fast chemical kinetic models are investigated to identify the reliable model for applications with a wide range of Mach numbers. Solutions from the Gardiner reaction-rate set, the Moss reaction-rate set, the Park rate set of 1993, and the Dunn and Kang reaction rate are compared. High-temperature, equilibrium-constant curve fits proposed by Gupta are also examined. The new Hansen's formulation for the rate controlling temperature for the dissociation reaction is compared with Park's approach. Particular attention has been devoted to backward reaction rates, because the methods of calculation affect the flowfield structure. Sample hypersonic flowfields, typical of spacecraft reentry conditions in which reactions play an important role, are presented and compared with results from experiments and other computational fluid dynamics simulations. The differences are discussed and evaluated.

Nomenclature

A_r	=	constant for forward reaction rate for reaction r
$A_{i,r}$, $a_{i,r}$	=	coefficient for equilibrium constant for reaction r
$K_{\text{eq},r}$	=	equilibrium constant for reaction r
$K_{f,r}$, $K_{b,r}$	=	forward and backward reaction-rate coefficient
$\hat{M}_i$	=	molecular weight of species i
r	=	reaction r
T	=	translational–rotational temperature
T_a	=	geometrically averaged temperature
T_{v_m}	=	vibrational temperature of molecule m
Z	=	coupling factor for vibration dissociation coupling process
$\alpha_{i,r}$	=	stoichiometric coefficient for reactant i in r
$\beta_{i,r}$	=	stoichiometric coefficient for product i in r
θ_r	=	characteristic temperature of reaction r
ρ	=	total density
ρ_i	=	density of species i
ω_i	=	mass production rate for species i

I. Introduction

THE efficient modern spacecraft design depends on having a precise understanding of the fluid dynamics, including the nonequilibrium chemical activity. The high temperature present for typically hypersonic flight conditions causes significant excitation of internal energy modes and provokes the dissociation of diatomic molecules and even ionization of the fluid. The variety of real gas effects that take place affects substantially the energy flux to the vehicle. The numerical simulation of hypersonic flow in thermochemical nonequilibrium past a blunt body presents considerable difficulties for accurate solutions in the stagnation region. Generally, efforts provided to solve these types of flows have been based on the full coupling between Navier–Stokes equations and the thermochemical phenomena. Many researchers have developed different chemical models for the description of hypersonic flowfields with the same experimental configurations. Therefore, it is important to determine an adequate model for the accurate description of hypersonic flowfields.

Some of the largest uncertainties in the modeling of reacting hypersonic flow are the chemical reaction rates and the coupling between thermochemical phenomena. The uncertainties about the thermochemical processes render calculations doubtful. Whereas methods for analyzing the aerodynamics in equilibrium flow have achieved a level of maturity, uncertainties remain in their nonequilibrium counterparts due to the incomplete modeling of chemical processes. Consequently, a good knowledge of the chemical modeling is required. For example, several chemical kinetic models give only the forward reaction rates. Many options are available for the calculation of the backward reaction rate with the equilibrium constant (Park [1], Gupta et al. [2], and Vincenti and Kruger [3]) and lead to different results. The method of computation of the backward reaction rate affects flowfield structures, shock shapes, and vehicle surface properties. It is necessary, therefore, to make a judicious choice of an adequate model through a comparative study.

In the literature, a multitude of models for chemical kinetics of air exist. These models are built on different simplifying assumptions, and all have advantages and disadvantages depending on the problem simulated. The objective of the present study is to investigate results obtained with four chemical reaction models. Solutions from models proposed by Gardiner [4], Shinn et al. [5], Dunn and Kang [6], and Park [7] are compared. Particular attention has been devoted to the way in which the backward reactions have been obtained. High-temperature least-squares equilibrium-constant curve fits are also included from Gupta et al. [2]. The influence of the formulations of Hansen [8] and Park [1] for the coupling between a molecule's vibrational state and its dissociation rate are compared. Several studies were presented in the past on the dissociation of nitrogen or of oxygen separately [9,10]. The extension of these works to the

Received 10 December 2008; revision received 22 April 2009; accepted for publication 22 April 2009.

*Assistant Professor of Fluid Mechanics, Institut Universitaire de Technologie Fotso Victor, Post Office Box 134; tchuengse@yahoo.com (Corresponding Author).

†Professor of Fluid Mechanics, Ecole Polytechnique Universitaire de Marseille, Department Mécanique Energénique, 5 rue Enrico Fermi Technopole de Chateau Gombert; David.Zeitoun@polytech.univ-mrs.fr. Senior Member AIAA.

complexity of overall reactions of air remains questionable. The present work attempts to identify the model with an acceptable confidence for a wide range of Mach number. One approach to validate the thermochemical model in computational fluid dynamics (CFD) codes is to compare the shock-standoff distance and the stagnation heating point along a sphere with the experimental data. The same CFD code is used to produce solutions.

An efficient and robust code for the computation of nonequilibrium flow, which has been extensively tested in the past [11,12], is used here for the solutions of the stagnation-region flowfield. The present scheme is based on a multiblock finite volume technique. The convective numerical flux is calculated by an upwind algorithm, based on artificially upstream flux vector splitting [12]. The second-order central differences are used to discretize the viscous fluxes. An accurate second-order algorithm in space and time is obtained by employing the MUSCL approach in conjunction with the minmod limiter and the time predictor–corrector schemes. The source terms are treated implicitly to relax the stiffness. The computation was performed in local time-stepping mode with a Courant–Friedrichs–Lewy (CFL) number of 0.8. The steady state is obtained after convergence of the unsteady formulation of the discretized equations. Convergence is achieved when the variation of total energy does not change more than 1% between two consecutive solutions of 1 time unit apart. The various upstream flow conditions for these computations are equivalent to those obtained in an experimental heat transfer study on blunt bodies conducted in a high enthalpy and hypervelocity expansion tube [11,13–15].

II. Analysis

The nonequilibrium hypersonic flow is assumed to be correctly described by a continuum formulation. The atmosphere is air or nitrogen and is assumed to be modeled by an ideal mixture of perfect gases involving five or two species. The governing equations are the two-dimensional Navier–Stokes equations. The code solves the mass conservation equations for each species (N, O, NO, O_2, and N_2 for air, and N and N_2 for nitrogen gas). The model includes a mass-average momentum equation in two directions, a total energy equation and a vibrational energy equation for each nonequilibrium molecule. The thermal nonequilibrium processes in the gas are accounted for with three temperature models (T, $T_{v_{O_2}}$, and $T_{v_{N_2}}$). The energy exchange between the translational and vibrational modes is described by the Landau–Teller theory, and the relaxation equations also take into account vibration dissociation coupling (CVD) coupling. The vibrational relaxation time is calculated using the correlation presented in [11].

For the viscous terms, the viscosity coefficient of each species is given by Blottner et al.'s model [16]. The thermal conductivity of each species is derived from Vincenti and Kruger's [3] relation and Wilke's semi-empirical mixing rule [17] is used to calculate the total viscosity and conductivity of the mixture. For the mass diffusion fluxes, the binary Lewis number is assumed to be the same, constant for all neutral species and equal to 1.2. The total heat flux is split between the contribution of the conduction flux of different internal modes and the diffusion of the total energy. A simple expression for the total heat flux, and more practical to handle, is established and facilitates the evaluation of the contribution of each mode of internal energy. The details of this model are presented in [11].

A. Chemical Processes

The accurate characterization of the shock layer in hypersonic flow requires good knowledge of the species mass, produced by chemical reactions that take place according to a suitable chemical kinetic model. An instantaneous accurate prediction of the mass fraction and the heating rate require a correct simulation of the chemical behavior of the flowfield. The mechanism by which the considered chemical reactions appear is little known. Several ways lead to intermediate products or highly unstable excited states, which are available virtually for each reaction. It is difficult to produce theoretical formulations that involve all species and to conduct experimental work for the kinetic data that shows the evolution of chemical reactions. Solutions from Dunn and Kang [6], Gardiner [4], Shinn et al. [5], and Park [7] reaction-rate sets are compared. All of these models are different essentially in the data of the forward and backward coefficients of reaction rates. In Dunn and Kang [6], the ratio of rate is not necessarily equal to the equilibrium constant as required by Eq. (2). A modified Dunn and Kang model is created when the backward rate is computed either with exact or curve-fit equilibrium constants. The different models taking into account only homogeneous reactions that involve the following reactions for air are as follows:

Dissociation

$$O_2 + M \rightleftharpoons O + O + M \qquad N_2 + M \rightleftharpoons N + N + M$$
$$NO + M \rightleftharpoons N + O + M$$

Exchange or Zel'dovich reaction

$$O + N_2 \rightleftharpoons NO + N \qquad NO + O \rightleftharpoons O_2 + N$$

M represents the collision partner which is one of the five species of the mixture.

For species i, the chemical source term ω_i is written

$$\omega_i = \hat{M}_i \sum_{r=1}^{NR} (\beta_{i,r} - \alpha_{i,r}) . \left[K_{f,r} \prod_{i=1}^{NS} \left(\frac{\rho_i}{\hat{M}_i} \right)^{\alpha_{i,r}} - K_{b,r} \prod_{i=1}^{NS} \left(\frac{\rho_i}{\hat{M}_i} \right)^{\beta_{i,r}} \right]$$

where NS and NR represent the total number of species and total number of reactions, respectively, and where the associated forward and reverse reaction-rate coefficients are assumed to satisfy the generalized Arrhenius law:

$$K_{f,r} = A_r T^{\eta_r} e^{-\theta_r / T} \tag{1}$$

Backward rates $K_{b,r}$ are defined either with curve-fit constants in the Arrhenius expression or with the equilibrium constant $K_{\mathrm{eq},r}$:

$$K_{\mathrm{eq},r} = \frac{K_{f,r}}{K_{b,r}} = \frac{\prod_{i=1}^{NS} (\rho_i / \hat{M}_i)^{\alpha_{i,r}}}{\prod_{i=1}^{NS} (\rho_i / \hat{M}_i)^{\beta_{i,r}}} \tag{2}$$

$K_{\mathrm{eq},r}$ can be determined analytically with the minimization of Gibb's free energy of each species under thermodynamics assumptions [3]. Moreover, for thermochemical nonequilibrium, the theoretical formulation becomes poorly defined due to the complexity of the physical phenomenon. However, the fitting of experimental data would be more reliable than the theoretical formulation, because every simplification introduced in the thermodynamics model affects results.

According to Park [7], the equilibrium constant $K_{\mathrm{eq},r}$ is given by the following exponential polynomial:

$$K_{\mathrm{eq},r} = \exp(A_{1,r} + A_{2,r} z + A_{3,r} z^2 + A_{4,r} z^3 + A_{5,r} z^4)$$
$$z = 10,000 / T \tag{3}$$

This Park curve fit was performed from data points only at 2000, 4000, 6000, 8000, and 10,000 K. Gupta et al. [2] have examined the curve fits for equilibrium constants to temperatures above 30,000 K. He demonstrates that the five parameters used in both the Park reaction-rate set [7] and those derived from the Dunn and Kang [6] rates are incorrect at temperatures above 10,000 K. Gupta et al.'s [2] least-squares curve fit, with a six parameter function for equilibrium constant, is of the form

$$K_{\mathrm{eq},r} = \exp(a_{1,r} z^5 + a_{2,r} z^4 + a_{3,r} z^3 + a_{4,r} z^2 + a_{5,r} z + a_{6,r}) \tag{4}$$

The forward reaction rates of the dissociation of the nitrogen molecule are represented in Fig. 1, and it is observed that the Dunn and Kang [6] kinetic is largely separated from the others. The influences of the equilibrium constants at the fast and the slow kinetic models (Park [7], Gardiner [4]) are shown in Fig. 2 with a large dispersion. The difference of calculation between analytic and curve fits of equilibrium constant can reach 10^6. The backward rate

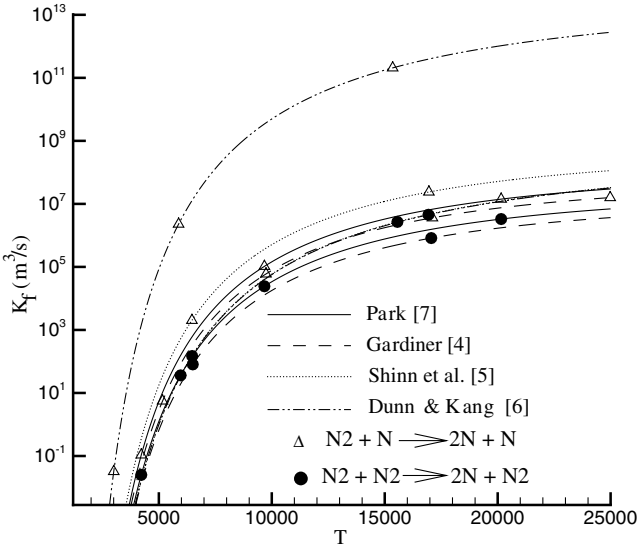

Fig. 1 Forward reactions rate.

constant with the Gupta et al. [2] curve fit are not monotonous. The causes of uncertainties in the determination of the reaction rates coefficients are multiple and are still rather poorly known. The present work examines various options for calculating the backward rates for several chemical kinetic models. The vibration–dissociation coupling is also considered in this paper.

B. Vibration–Dissociation Coupling

The vibration–dissociation coupling is very important behind a strong shock in thermochemical nonequilibrium flow. Directly behind the shock, the translational temperature reaches a maximum value, whereas the vibrational temperature takes time to be excited before reaching its equilibrium value. Therefore, a model of dissociation depending only on the translational temperature will tend to overestimate total dissociation. The most important and poorly understood issue is how to model the coupling between a molecule's vibrational state and its dissociation rate. Many analyses of this coupling have been made in the past, either with more or less realistic and sophisticated physicochemical models, or with semi-empirical methods easily usable in hypersonic computation codes [1]. There are perhaps 10 such models available in literature, however, only the Park [7] and Hansen [8] models are used in this study.

Chemical reaction rates are affected by the extent to which the internal modes of atoms and molecules are excited. The coupling

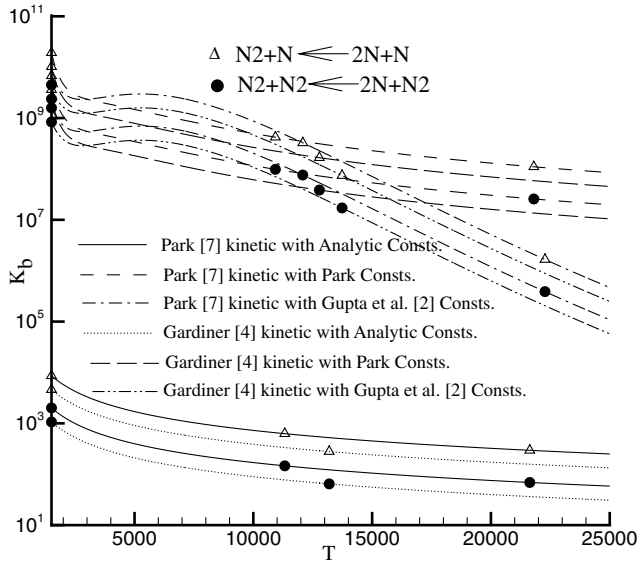

Fig. 2 Backward reactions rate.

Table 1 CVD coefficients for Hansen's [8] model

	α	β
N_2	0.90	0.30
O_2	0.85	0.25
NO	0.80	0.30

factor translating the influence of the vibration on dissociation is given by the ratio

$$Z(T, T_v) = \frac{K_f(T, T_v)}{K_f(T)} \tag{5}$$

There are several methods for including thermal nonequilibrium effects in the chemical kinetic of air. Some have a semi-empirical origin, based on experimental results, and are often extrapolated well beyond their validity domains (without physical justification). Whereas those with analytical origin arise from particle collision theory. Park [1] suggested a geometrically averaged rate controlling temperature T_a for dissociation reactions. T_a is defined as

$$T_a = T^q T_{v_m}^{1-q} \quad \text{and} \quad K_{f,r}(T, T_{v_m}) = A_r T_a^{\eta_r} e^{-\theta_r/T_a} \tag{6}$$

with $q = 0.5$ in the original formulation. Sharma et al. [18] suggested that the value of q varied from 0.6 to 0.7 might be more realistic for high-enthalpy flow and, consequently, a value of 0.7 is used in the present study. Sharma et al.'s modification of the model is based on the analysis of experimental data for the reaction velocity observed in shock tubes. Hansen [8] used collisional cross section theory to compute dissociation reaction rates up to 40,000 K for flow in thermal nonequilibrium. He suggested an alternative formulation for the rate controlling temperature, similar to the Park approach [1],

$$q = \alpha - \beta\left(\frac{T_v}{T}\right) \tag{7}$$

with α and β values reported in Table 1.

The various values of the coupling factor for O_2 and N_2 at $T = 20,000$ K are represented in Fig. 3. Shatalov and Losev's [19] coupling is also included. As evident in Fig. 3, the magnitude of the coupling is very sensitive to the coupling model used.

III. Results and Discussions

A. Boundary Conditions

The grid points used in calculations are densely distributed near the wall and near the position of the shock wave, as plotted in Fig. 4.

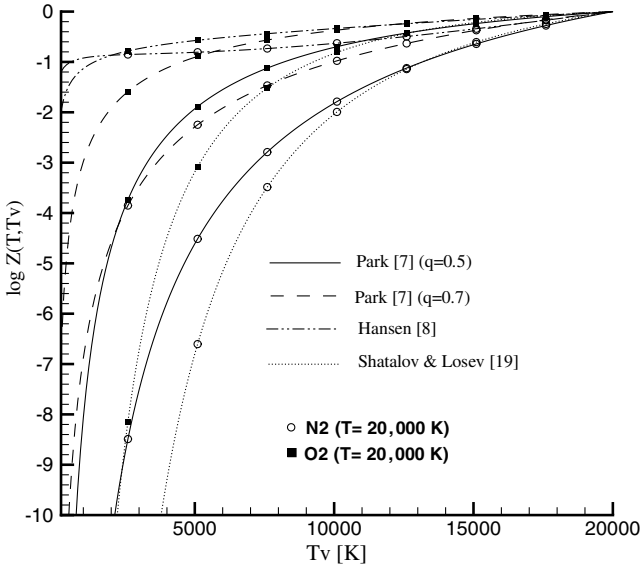

Fig. 3 Coupling factor $Z(T, T_v)$ for O_2 and N_2.

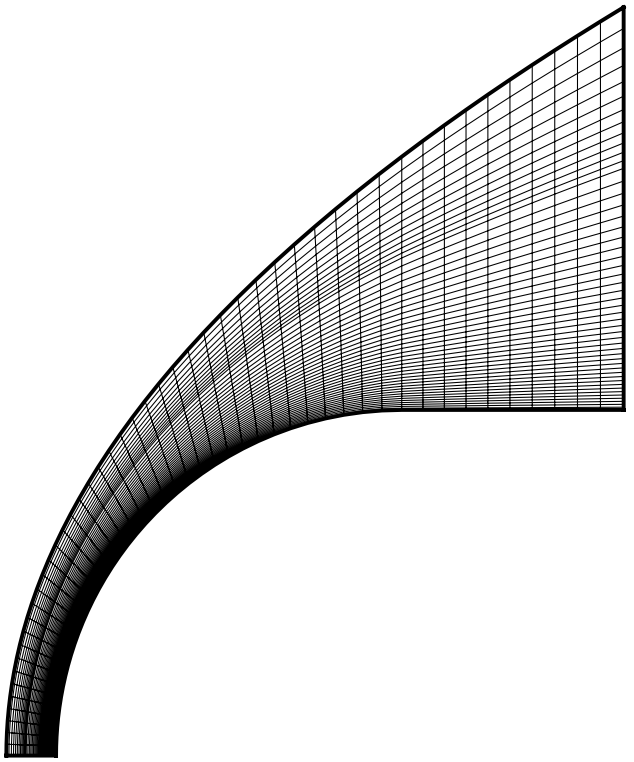

Fig. 4 Computational grid 50 × 50.

The upstream flow conditions, the number of nodes, and the minimum grid spacing in x and y directions considered in this study are reported in Table 2. The time step is computed locally in each cell from a given CFL number. The boundary conditions are imposed along the wall. The wall temperature T_w is fixed. The no-slip and no-temperature jump conditions are used. The freestream condition is hypersonic. The outflow is supersonic and the zero gradient exit condition is appropriate. Along the stagnation line, the flowfield is symmetric. A noncatalytic wall is assumed in all of the present calculations. Also, the freestream Reynolds numbers are calculated with the length scale equal to the nose radius, sphere, or cylinder as appropriate. In each case, the freestream air/nitrogen gas is composed of 79% N_2 and 21% O_2 or 92.7% N_2 and 7.3% N.

B. Conditions of Numerical Simulation

The computational results are validated with experimental observations reported by Lobb [13], Rose and Stankevics [14], and Hornung [15] for the shock-standoff distance and surface heat transfer distributions. Results of the current numerical simulations are validated with the shock-tunnel data presented in Table 2.

The first case study involves Lobb's experiment [13] devoted to the measure of shock detachment at 5.28 km/s. The second computation is also validated with the shock-tube measurements of the stagnation point heat flux for blunt bodies at 5.74 km/s from the work of Rose and Stankevics [14]. The RAM-CII flight is a program conducted by the NASA Langley Research Center to assess the effects of blackout during reentry. Computations were performed for RAM-CII conditions at Mach 25.9 for comparison with available numerical simulations. For the last case that involved hypersonic nitrogen flow over cylinders, the focus was to reconstruct the interferogram experiments performed by Hornung [15]. The results have been found to compare favorably with experimental results obtained with a free-piston-driven shock-tube wind tunnel, which was used to obtained interferograms of the flow of pure nitrogen over blunt-nosed bodies.

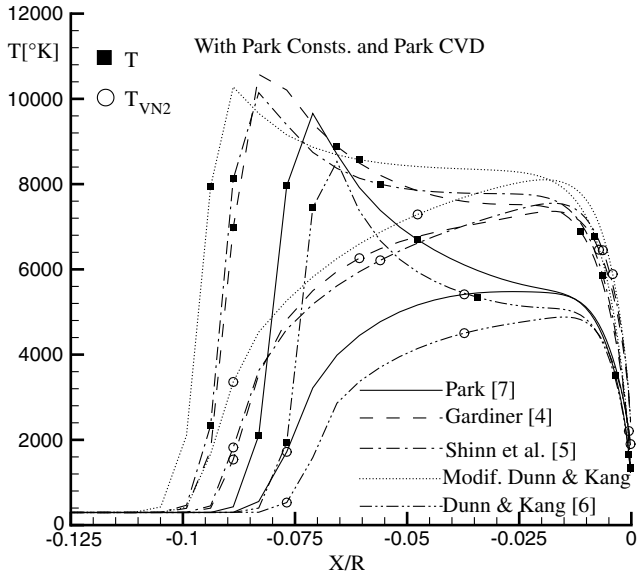

Fig. 5 Temperatures along the stagnation line, $M_\infty = 15.3$.

A grid resolution study was performed in our former work [12] to determine the number of points required for different cases. The current numerical algorithm was used to achieve grid independent solutions and for a flow in thermochemical nonequilibrium. The same CFD code and mesh points are used to examine the influence of all the current chemical kinetic models selected on flowfield structures, shock shapes, and vehicle surface properties. The results obtained are presented and compared with experimental data and numerical results.

C. Lobb's Experiment

The predicted temperatures distribution along the stagnation streamline of T and $T_{v_{N_2}}$ for five chemical models are shown in Fig. 5. The computations are done with Park curve-fit equilibrium constants in conjunction with Park CVD coupling [7]. The maximum value of T and $T_{v_{N_2}}$ behind the shock wave is obtained with the slow kinetic

Table 2 Detail of freestream conditions and grids used

Experiments	Lobb [13]	Rose and Stankevics [14]	Ram-CII [11]	Hornung [15]
Gas	Air	Air	Air	N_2, N
R_s, mm	6.35	6.6	152.4	0.5 in.
M_∞	15.3	18	25.9	6.14
U_∞, m/s	5263	5742.49	7658.6	5590
P_∞, Pa	664	432.2	4.764	2910
T_∞, K	293.0	252	216	1833
T_{wall}, K	1000	555.5	1500	adiabatic
R_{e_∞}	14,605	12,840	6280	6000
IM nodes	50	60	70	50
JM nodes	50	60	70	50
$\Delta x_{\min}$, m	4.1936×10^{-6}	1.423×10^{-6}	2.002×10^{-5}	4.214×10^{-5}
$\Delta y_{\min}$, m	7.2055×10^{-5}	4.6432×10^{-5}	1.27×10^{-4}	1.072×10^{-4}

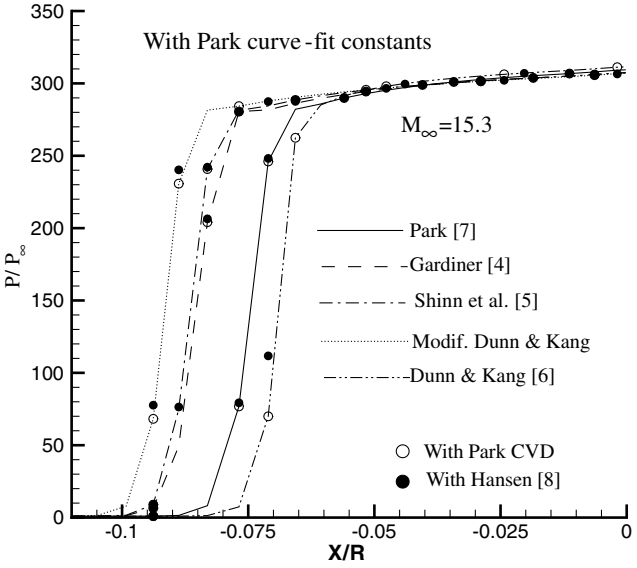

Fig. 6 Pressure distribution along the stagnation line, $M_\infty = 15.3$.

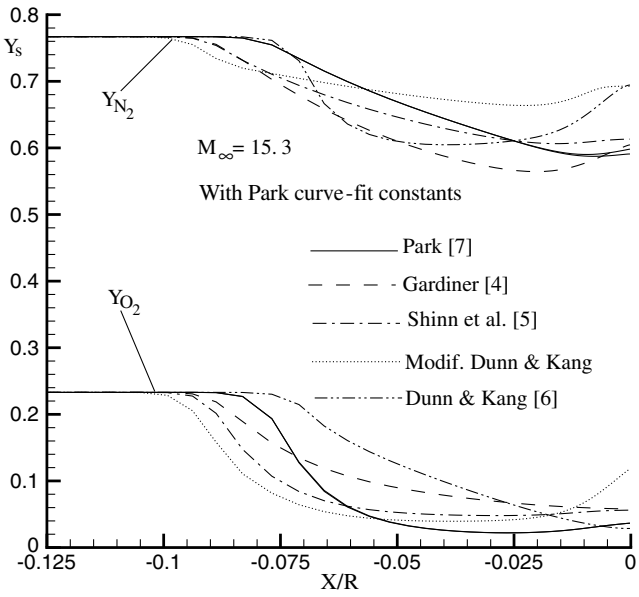

Fig. 7 Mass fractions, Y_{N_2} and Y_{O_2}, $M_\infty = 15.3$.

models. It is clearly seen that the vibrational relaxation time for molecular nitrogen in the postshock region is greatest with the slow kinetic models and lowest with the fast kinetic models, caused by higher density in the shock layer, which enhances the collisional energy transfer mechanisms. It is observed that all temperatures tend toward a thermodynamic equilibrium near the stagnation point. Note that the features of the flow physics are evident by the existence of a significant thermal nonequilibrium behind the shock wave, and the vibrational temperature remains below the associated translational temperature whatever the choice of chemical kinetic model. The original Dunn and Kang [6] model predicts the lowest temperatures which become as high as the Gardiner prediction [4] when the backward rates are calculated with the Park equilibrium constant [7].

The predicted pressure distributions along the stagnation line are plotted in Fig. 6. It is noted that all chemical models converge to the same peak value of pressure at the stagnation point, and that the difference between the Hansen [8] and Park CVD coupling [7] cannot be discriminated. These distributions are used to identify the shock location. One can see that the shock-standoff distance tends to increase when the kinetic velocity is decreased, approaching the frozen flow. The shock-standoff distance is the smallest for the case of fast kinetic models, suggesting a higher degree of dissociation compared to other kinetics. The peak temperature, however, is highest for Gardiner model [4] and lowest for the Dunn and Kang model [6], as expected. A comparison with the location given by Lobb [13] is reported in Table 3. The values reported for the shock-standoff distance correspond to the point of the maximum pressure gradient associated with the thickness of the mesh. With respect to the shock-standoff distance observed in the Lobb experiment (0.087 R_s with a $\pm 5.75\%$ experimental uncertainty), the calculated standoff value predicted using Park's [7] data is 4.36% smaller, whereas the value predicted with the Gardiner data [4] is 7.46% greater. The result produced by the Park [7] model is closest to the experimental value.

The evolutions of the mass fractions have a dependence on the choice of the model employed. Figure 7 presents a comparison of the trace of the dissociation of N_2 and O_2 across the stagnation region, resulting from the five chemical reaction models. Park CVD coupling [7] is used in all five calculations. The evolutions are distinct, and therefore the calculated wall heat flux presented in Fig. 8 as a function of the angle θ is affected. The fast kinetic models produce similar profiles. The same observation is made with the slow kinetic models. At the stagnation point, the current chemical models produce stagnation heating values that range from 23 to 38 MW/m^2. The calculation of the backward reactions with the analytic equilibrium constant tends to increase the wall heat flux with Park's model [7], whereas Gardiner's model [4] tends to decrease it about 13 MW/m^2 at the stagnation point. The numerical results obtained by other authors are about 25 MW/m^2 [20,21]. This case demonstrates that the Park model [7] with a Park curve-fit constant has a better prediction of shock-standoff distance and wall heat flux value.

Table 3 Shock standoff distance, $M_\infty = 15.3$

With Park consts. [7]	δ/R, %
Park [7]	8.321
Gardiner [4]	9.349
Shinn et al. [5]	9.35
Modified Dunn and Kang	9.930
Dunn and Kang [6]	7.650
Lobb, experiment [13]	**8.7 ± 0.5**

D. Rose and Stankevics's Experiment

Calculations for the second case focus on the Mach 18 air experimental case of Rose and Stankevics [14] (Table 2). Computed temperature distributions obtained with the Park model [7] along the stagnation line are shown in Fig. 9. The backward reaction rates are evaluated either with analytic or Park and/or Gupta et al. [2]

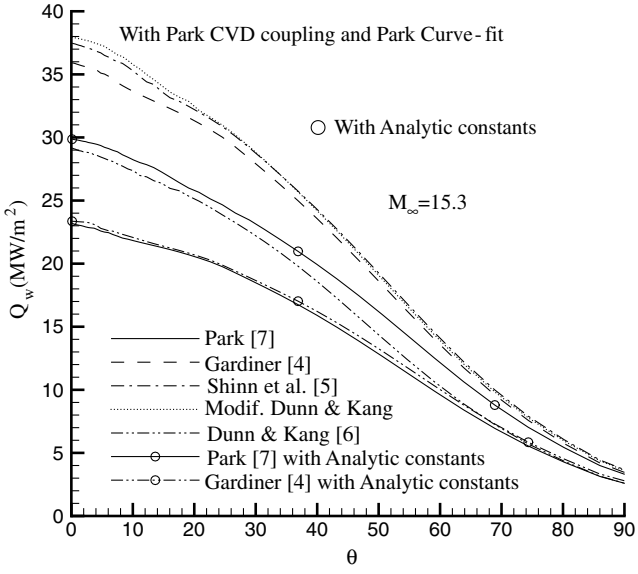

Fig. 8 Wall heat flux, $M_\infty = 15.3$.

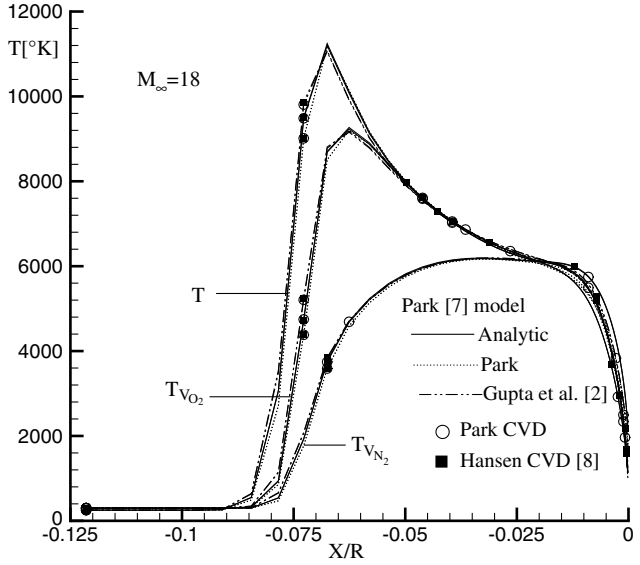

Fig. 9 Temperatures with Park [7] model, $M_\infty = 18$.

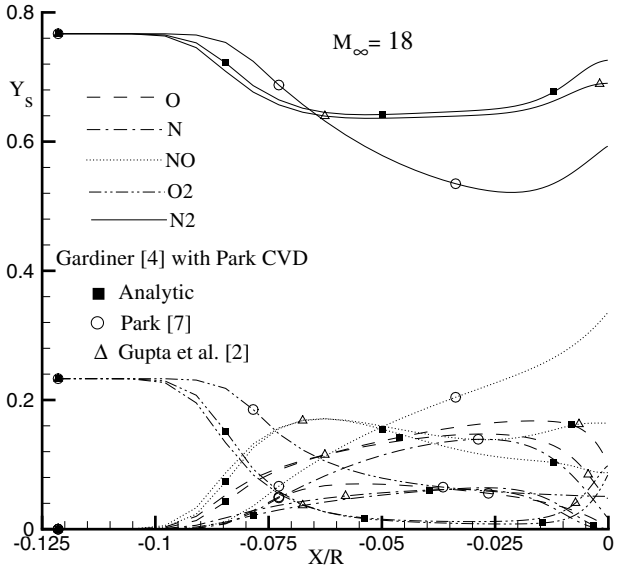

Fig. 11 Mass fraction profiles with Gardiner reactions [4], $M_\infty = 18$.

equilibrium constants. In the Park [7] model, the manner in which the backward reaction rates are calculated do not affect profiles. The nonequilibrium behavior of the vibrational energy mode can be seen from the temperature profiles near the shock region. It can be seen from the variation of the vibrational temperatures in the vicinity of the shock wave that the vibrational relaxation time for O_2 is the lowest. This figure clearly shows that the influences of the CVD coupling of Park [7] and Hansen [8] are not visible in the Park [7] model. The evolution of temperatures obtained with the Gardiner [4] model presented in Fig. 10 are affected by the method of computation of the backward reactions. Note that the same observation applies to the Mach 15.3 case where the temperatures obtained with the slow kinetic models behind the shock wave are high.

The mass fraction distribution across the stagnation streamline are plotted in Figs. 11 and 12. Figure 11 shows Gardiner's model [4], with Park CVD coupling [7]. The computations with Park and Gupta et al.'s [2] curve-fit equilibrium constants are inconsistent in the vicinity of the stagnation point. The evolutions are distinct with a great dissociation of the N_2 molecule behind the shock wave when Park curve-fit equilibrium constants are used [7]. The formation of NO does not exhibit consistent behavior. Nitric oxide concentration in the vicinity of the shock wave and near the wall is the highest for the case with Park curve-fit constants. Evident near the stagnation point is the relatively close agreement in the results provided by the analytic and Gupta et al.'s [2] processing of the backward rates, both of which differ from the Park treatment [7]. The equilibrium curve-fit constants of Park suffer at low temperatures when the gas is not chemically reactive. The wall temperature is very low (555.5 K) in this case. Figure 12 shows the mass fraction with Park's [7] model. The three backward reactions predict similar dissociation distances, as has been noted with temperature distributions. A large difference in Park's [7] model is observed near the wall. The temperature is weak with a great recombination of the N_2 molecule for the use of analytic constant equilibrium. The distinct evolution near the surface has an influence on the wall heat flux.

It is important to determine the correct dissociation rate in hypersonic flow, because the degree of dissociation significantly affects the heat transfer when the surface is catalytic with recombination of atoms (as is the case for most thermal protection materials). Figure 13 shows the heat transfer Q_w along the body surface for four chemical kinetic models. As expected, the higher values of Q_w are obtained with slower kinetics. The stagnation point heat transfers are reported in Table 4 and compared with experimental data [14]. Computed stagnation heat flux is overpredicted with Gardiner [4], Shinn et al. [5], and modified Dunn and Kang models. In the attempt to improve the Dunn and Kang model [6], a modified Dunn and Kang model was obtained by using equilibrium

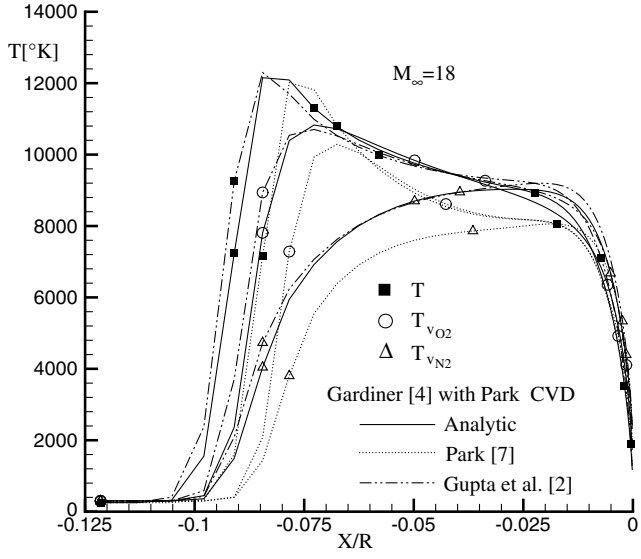

Fig. 10 Temperatures profile with Gardiner [4] model, $M_\infty = 18$.

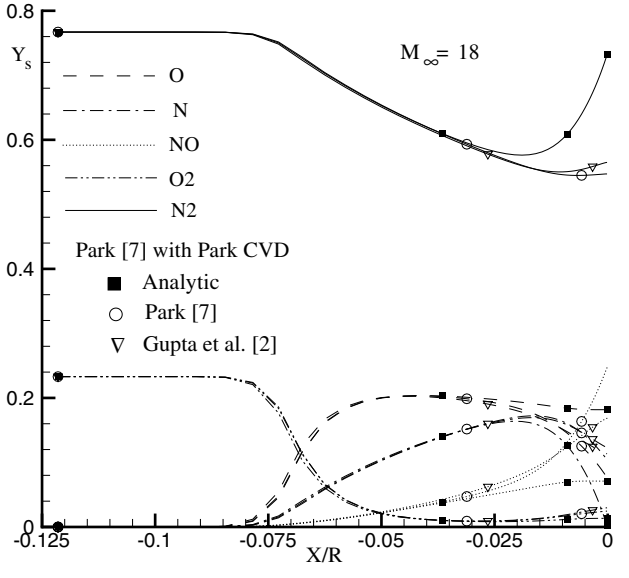

Fig. 12 Mass fraction with Park [7] reactions, $M_\infty = 18$.

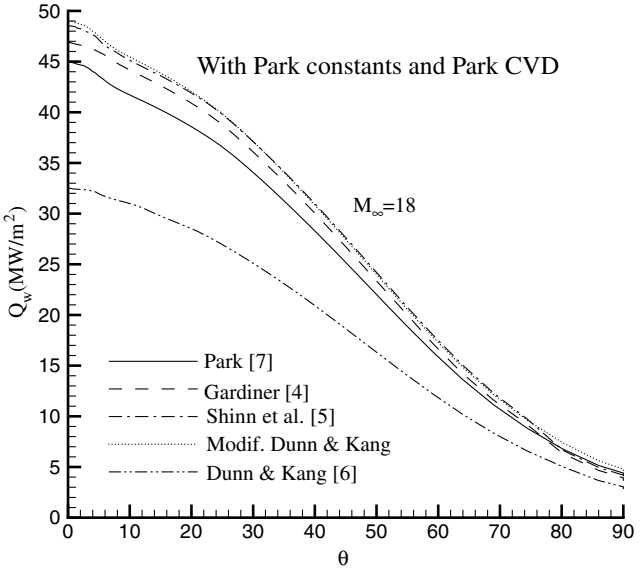

Fig. 13 Wall heat flux, $M_\infty = 18$.

constants in the calculation of the backward reactions. The model of Park [7] gives better agreement with the experimental measurement.

E. RAM-CII Experiment

Although there are no experimental measurements of heat flux in the present case, the interest of this study is to submit the chemical models to very high temperatures and to compare numerical results. The graphs presented here are obtained with the Gupta et al. [2] equilibrium constant for which the field of validity is wider.

In Fig. 14, the translational temperature is around 20,000 K and the extrapolation of certain formulations becomes erroneous. For example, at this temperature, it is necessary to account for ionization, although the chemistry of Gardiner [4] and Shinn et al. [5] is conceived only for neutral air gas. There is a significant decrease in the temperature predicted by the modified Dunn and Kang model. These differences indicate that the Dunn and Kang rate set [6] is not consistent with Gupta et al.'s [2] equilibrium constants at the higher temperatures associated with Mach 25.9. This conclusion is easily verified for each reaction with a direct comparison of the equilibrium constants to the ratio of rates. Inconsistency with Gupta's equilibrium constants does not ensure that Dunn and Kang [6] rates will not produce correct species distributions. This inconsistency, however, raises doubt as to recommending this rate set as the correct data for these flows.

The evolution of the species O_2 and N_2 are represented in Fig. 15. It is observed that the greatest dissociation of N_2 behind the shock wave and a strong recombination near the stagnation point is obtained with the Dunn and Kang model [6]. For O_2, the trend of the curves is similar. Behind the shock wave, it is noted that the complete dissociation of O_2 is obtained with all models. The concentration of N_2 near the stagnation point is highest (around 62%) for the slow kinetic models and lowest (around 41%) for the fast kinetic models. It is due to this reason that differences in surface heat transfer exist for different kinetics.

Table 4 Stagantion heat flux Q_w (MW/m^2), with Park CVD coupling [7], Mach 18

Chemical kinetics with K_{eq}	Park [7]	Gupta et al. [2]
Park [7]	44.95	45.5
Gardiner [4]	47.0	47.4
Shinn et al. [5]	48.5	49.2
Modified Dunn and Kang	49.0	50.1
Dunn and Kang [6]		32.5
Fay and Ridell [22]		**45.0**
Rose and Stankevics, experiment [14]		**46.0**

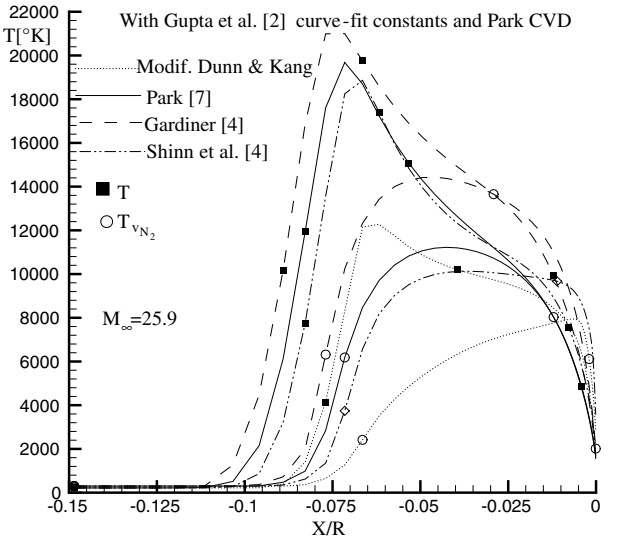

Fig. 14 Temperature profile with Gupta et al. [2] curve-fit constants, $M_\infty = 25.9$.

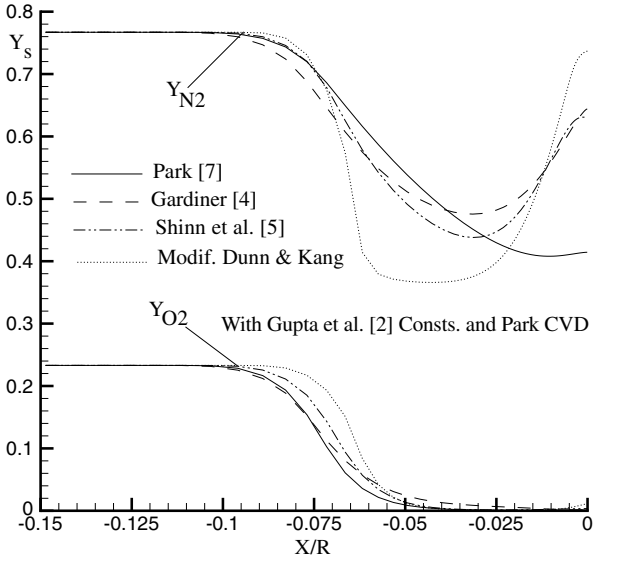

Fig. 15 Mass fraction profile with Gupta et al. [2] curve-fit constants, $M_\infty = 25.9$.

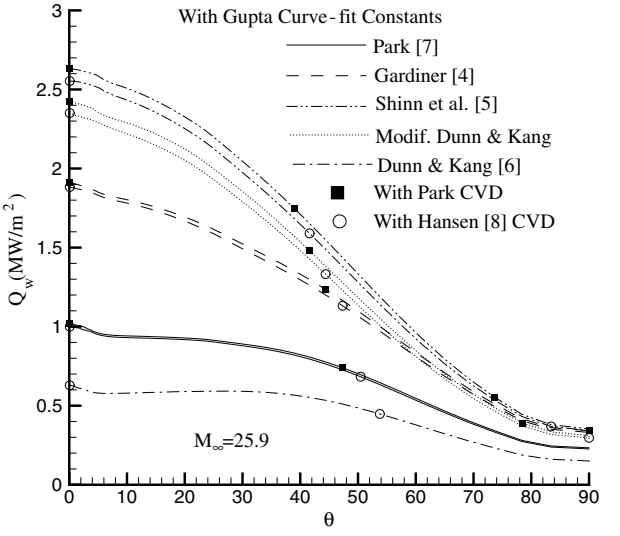

Fig. 16 Stagnation heat flux, $M_\infty = 25.9$.

Table 5 Stagnation heat flux, RAM-CII, Mach 25.9

Source	Chemical model	Q_w, MW/m^2
Present	Dunn & Kang [6]	0.58
Present	Park [7]	1.02
Present	Gardiner	1.91
Present	Dunn & Kang [6] plus Gupta et al. [2]	2.42
Present	Shinn et al. [5]	2.63
Walpot [23]	Park [7]	**0.74**
Walpot [23]	Dunn & Kang [6]	**0.90**
Soubrié et al. [24]	Park [7]	**0.96**
Candler & MacCormack [25]	Park & Wray	**2.5**

The surface heat transfer Q_w is shown in Fig. 16 for four chemical kinetic models. The difference of peaks between calculations with Park CVD coupling [7] and Hansen [8] at the stagnation point is about 2.5%. The maximum value of the heat flux is located at the position $\theta = 0$ deg. The computed stagnation point heat flux results are compared with other numerical results in Table 5. The large dispersion of the results obtained puts into doubt the accuracy of certain reaction rates or indicates that some other unknown thermochemical process occurs in these flows. The numerical results reported in Table 5 are obtained with a noncatalytic wall. The numerical methods and the selected chemical model are different. Walpot [23] and Soubrié et al. [24] have used a model with 11 species, whereas a model with 7 species has been considered by others [12,25]. The flux value for Candler and MacCormack [25], given in Table 5, is estimated from the Stanton number. It is noted that the values obtained with the slow kinetic models are higher. This was encountered in all the cases that were studied. Moreover, in former work [11], the present air code using the Park [7] chemical ionized model predicts with good accuracy the measured peak electron number density along the body for Mach 25.9.

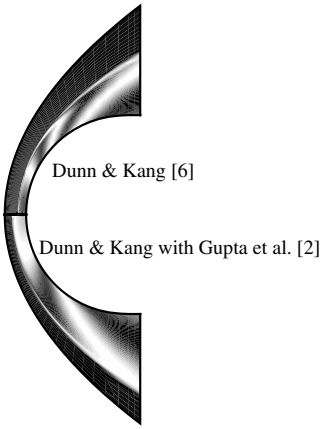

Fig. 17 Dunn and Kang [6] and modified Dunn and Kang interferograms computed.

F. Hornung's Experiment

Calculations involving hypervelocity nitrogen flow over cylinders are performed under conditions reported in Table 2. The results obtained demonstrate the sensitivity of the flowfield to the effect of finite rate chemistry. The freestream gas is composed of nitrogen dissociated partially ($Y_{N_2} = 0.927$, $Y_N = 0.073$). The wall is assumed to be adiabatic and noncatalytic. This case implements the experiment performed by Hornung [15] for 1-in.-diam cylinders with the dissociation of nitrogen at 5.59 km/s. The calculations use three different sets of dissociation rates of N_2.

The calculations using the corresponding freestream conditions have been made for the body, and Figs. 17–20 show interferograms and computed fringe patterns derived from the simulation results.

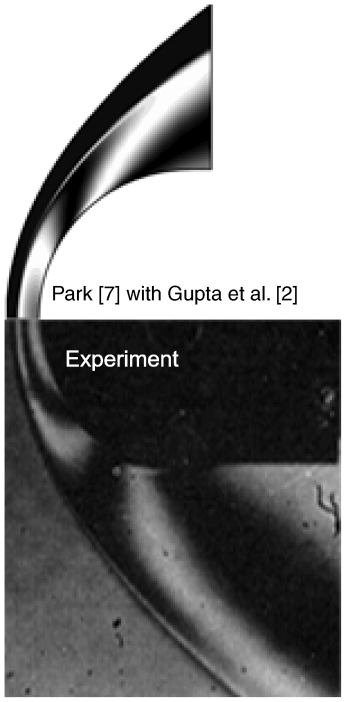

Fig. 18 Fringe patterns on 1-in.-diam cylinder with Park [7] model and Gupta et al. [2] equilibrium constant.

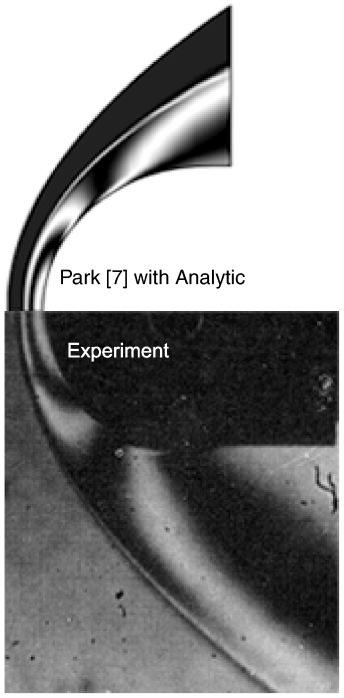

Fig. 19 Fringe patterns on 1-in.-diam cylinder with Park [7] model and exact equilibrium constant.

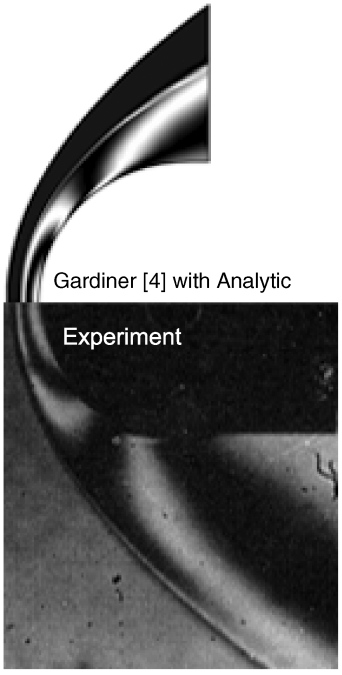

Fig. 20 Fringe patterns on 1-in.-diam cylinder with Gardiner [4] model and exact equilibrium constant.

The exact position of the shock in both the experiments and the simulations is uncertain: in the experiments, because of the shock curvature in the transverse direction, and in the simulations, because the shock is smeared over a few cell widths. To compare the experiments and the simulations more closely, it is necessary to compare fringe shifts at different locations in the flow. Figure 17 compares the computed interferograms obtained with Dunn and Kang [6] and the modified Dunn and Kang models. In the modified model, the backward rates are calculated with the Gupta et al. [2] curve-fit equilibrium constant. The two solutions are quite different. The distance from the detachment of the shock is sensitive to the chemical model selected. Although the Dunn and Kang model [6] is very poor, the modified version improves the thickness of the shock layer and makes it identical to the result obtained by the Park [7] model with Gupta et al.'s [2] equilibrium constant. The results produced by Park's [7] model with Gupta et al.'s [2] equilibrium constant are presented in Fig. 18 and compared with the experimental interferogram. It is observed that this computation cannot qualitatively reproduce the experiment.

The fringes for the case with Park [7] and Gardiner [4] with analytic equilibrium constant are plotted in Figs. 19 and 20. The frames are quantitatively well predicted. The experimental and computational interferograms have the same general features, but differ little in the details. The best comparison is obtained with the Park [7] model.

IV. Conclusions

The hypersonic flow past blunt bodies with thermochemical nonequilibrium was numerically simulated. The dependence of solutions on available chemical models, allowing one to assess the accuracy of finite rate chemical processes, has been examined. The present results were successfully validated with the theoretical and experimental work for shock-standoff distances, stagnation point heat transfer, and interferograms of the flow. Although all models describe the essential aspects of the nonequilibrium zone behind the shock, they are not accurate for the evaluation of the aerothermodynamic parameters. A comparative study of various kinetic air models is carried out to identify the reliable models for applications with a wide range of Mach number.

The present study has shown that the prediction of hypersonic flowfield structures, shock shapes, and vehicle surface properties are very sensitive to the choice of the kinetic model. The large dispersion in the wall heat flux reaches 60% as observed in the RAM-CII case. The manner in which the backward reaction rates are computed is quite important, as indicated by the interferograms that were obtained. The model of Park [7] gives a better prediction of the hypersonic flowfield. The Hansen [8] and the Park [7] CVD coupling for dissociation rate controlling temperature are shown to have negligible effects. Park [7] is identified as the model with a confidence acceptable to a wide range of Mach number.

Further research is required for the study of wall catalytic effects and to determine how large the influence of the wall temperature is on the computed shock-standoff distances and wall heat flux in the different kinetic models.

References

[1] Park, C., "Assessment of Two Temperature Kinetic Model for Ionizing Air," *Journal of Thermophysics and Heat Transfer*, Vol. 3, No. 3, 1989, pp. 233–244. doi:10.2514/3.28771

[2] Gupta, R. N., Yos, J. M., Thompson, R. A., and Lee, K. P., "A Review of Reaction Rates and Thermodynamic and Transport Properties for an 11-Species Air Model for Chemical and Thermal Nonequilibrium Calculations to 30,000 K," NASA RP-1232, 1990.

[3] Vincenti, W. G., and Kruger, C. H., Jr., "Introduction to Physical Gas Dynamics," Krieger, Malabar, FL, 1965.

[4] Gardiner, W. C., *Combustion Chemistry*, Springer–Verlag, Berlin, 1984.

[5] Shinn, J. L., Moss, J. N., and Simmonds, A. L., "Viscous Shock Layer Heating Analysis for the Shuttle Winward Plane Finite Recombination Rates," AIAA Paper 82-0842, 1982.

[6] Dunn, M. G., and Kang, S. W., "Theoretical and Experimental Studies of Re-Entry Plasma," NASA CR-2232, 1973.

[7] Park, C., "Review of Chemical-Kinetic Problems of Future NASA Mission, I: Earth Entries," *Journal of Thermophysics and Heat Transfer*, Vol. 7, No. 3, 1993, pp. 385–398. doi:10.2514/3.431

[8] Hansen, C. F., "Vibrational Nonequilibrium Effect on Diatomic Dissociation Rates," *AIAA Journal*, Vol. 31, No. 11, 1993, pp. 2047–2051. doi:10.2514/3.11889

[9] Macrossan, N. M., "Hypervelocity Flow of Dissociating Nitrogen Downstream of a Blunt Nose," *Journal of Fluid Mechanics*, Vol. 217, No. 1, 1990, pp. 167–202. doi:10.1017/S0022112090000672

[10] Josyula, E., "Oxygen Atoms Effect on Vibrational Relaxation of Nitrogen in Blunt Body Flows," *Journal of Thermophysics and Heat Transfer*, Vol. 15, No. 1, 2001, pp. 106–115. doi:10.2514/2.6585

[11] Tchuen, G., and Zeitoun, E. D., "Computation of Thermochemical Nonequilibrium Weakly Ionized Air Flow over Sphere Cones," *International Journal of Heat and Fluid Flow*, Vol. 29, No. 5, 2008, pp. 1393–1401. doi:10.1016/j.ijheatfluidflow.2008.06.002

[12] Tchuen, G., Burtschell, Y., and Zeitoun, E. D., "Computation of Non-Equilibrium Hypersonic Flow with Artificially Upstream Flux Vector Splitting (AUFS) Schemes," *International Journal of Computational Fluid Dynamics*, Vol. 22, No. 4, 2008, pp. 209–220. doi:10.1080/10618560701766525

[13] Lobb, K., "Experimental Measurement of Shock Detachment Distance on Sphere Fired in Air at Hypervelocities," *The High Temperature Aspect of Hypersonic Flow*, edited by W. C. Nelson, Macmillan, New York, 1964.

[14] Rose, P. H., and Stankevics, J. O., "Stagnation-Point Heat Transfer Measurements in Partially Ionized Air," *AIAA Journal*, Vol. 1, No. 12, 1963, pp. 2752–2763. doi:10.2514/3.2169

[15] Hornung, H. G., "Non-Equilibrium Dissociating Nitrogen Flow over Spheres and Circular Cylinders," *Journal of Fluid Mechanics*, Vol. 53, No. 1, 1972, pp. 149–176. doi:10.1017/S0022112072000084

[16] Blottner, F. G., Johnson, M., and Ellis, M., "Chemically Reacting Viscous Flow Program for Multi-Component Gas Mixtures," Sandia Lab., Albuquerque, NM, Rept. Sc-RR-70-754, 1971.

[17] Wilke, C. R., "A Viscosity Equation for Gas Mixture," *Journal of Chemical Physics*, Vol. 18, No. 4, 1950, pp. 517–519. doi:10.1063/1.1747673

[18] Sharma, S. P., Huo, W. M., and Park, C., "The Rate Parameters for Coupled Vibration-Dissociation in a Generalized SSH Approximation Flows," AIAA Paper 88-2714, 1988.

[19] Shatalov, O. P., and Losev, S. A., "Modeling of Diatomic Molecules Dissociation Under Quasistationary Conditions," AIAA Paper 97-2579, 1997.

[20] Joly, V., Coquel, F., Marmignon, C., Aretz, W., Metz, S., and Wilhelmi, H., "Numerical Modelling of Heat Transfer and Relaxation in Nonequilibrium Air at Hypersonic Speeds," *La Recherche Aérospatiale*, No. 3, 1994, pp. 219–234.

[21] Séror, S., Schall, E., and Zeitoun, E. D., "Comparison Between Coupled Euler/Defect Boundary-Layer and Navier–Stokes Computations for Nonequilibrium Hypersonic Flows," *Computers & Fluids*, Vol. 27, No. 3, 1998, pp. 381–406. doi:10.1016/S0045-7930(97)00072-8

[22] Fay, J. A., and Riddell, F. R., "Theory of Stagnation Point Heat Transfer in Dissociated Air," *Journal of the Aeronautical Sciences*, Vol. 25, No. 2, 1958, pp. 73–85.

[23] Walpot, L. M., "Development and Application of a Hypersonic Flow Solver," Ph.D. Thesis, Delft Univ. of Technology, Delft, The Netherlands, 2002.

[24] Soubrié, T., Rouzaud, O., and Zeitoun, E. D., "*Computation of Weakly Multi-Ionized Gases for Atmospheric Entry Using an Extended Roe Scheme*," European Community on Computational Methods in Applied Sciences, Jyväskylä, Finland, 2004.

[25] Candler, V. G., and MacCormack, W. R., "The Computation of Hypersonic Ionized Flows in Chemical and Thermal Nonequilibrium," AIAA Paper 88-0511, 1988.